Environmental Science & Technology

pubs.acs.org/est

Article

Zinc Stable Isotope Fractionation Mechanisms during Adsorption on and Substitution in Iron (Hydr)oxides

Xinran Yan, Wei Li, Chuanwei Zhu, Caroline L. Peacock, Yizhang Liu, Hui Li, Jing Zhang, Mei Hong, Fan Liu, and Hui Yin*

Cite This: *Environ. Sci. Technol.* 2023, 57, 6636−6646

Read Online

ACCESS | Metrics & More | Article Recommendations | Supporting Information

ABSTRACT: The Zn isotope fingerprint is widely used as a proxy of various environmental geochemical processes, so it is crucial to determine which are the mechanisms responsible for isotopic fractionation. Iron (Fe) (hydr)oxides greatly control the cycling and fate and thus isotope fractionation factors of Zn in terrestrial environments. Here, Zn isotope fractionation and related mechanisms during adsorption on and substitution in three FeOOH polymorphs are explored. Results demonstrate that heavy Zn isotopes are preferentially enriched onto solids, with almost similar isotopic offsets ($\Delta^{66/64}Zn_{solid\text{-}solution}$ = 0.25−0.36‰) for goethite, lepidocrocite, and feroxyhyte. This is consistent with the same average Zn−O bond lengths for adsorbed Zn on these solids as revealed by Zn K-edge X-ray absorption fine structure spectroscopy. In contrast, at an initial Zn/Fe molar ratio of 0.02, incorporation of Zn into goethite and lepidocrocite by substituting for lattice Fe preferentially sequesters light Zn isotopes with $\Delta^{66/64}Zn_{substituted\text{-}stock\ solution}$ of −1.52 ± 0.09‰ and −1.18 ± 0.15‰, while Zn-substituted feroxyhyte (0.06 ± 0.11‰) indicates almost no isotope fractionation. This is closely related to the different crystal nucleation and growth rates during the Zn-doped FeOOH formation processes. These results provide direct experimental evidence of incorporation of isotopically light Zn into Fe (hydr)oxides and improve our understanding of Zn isotope fractionation mechanisms during mineral−solution interface processes.

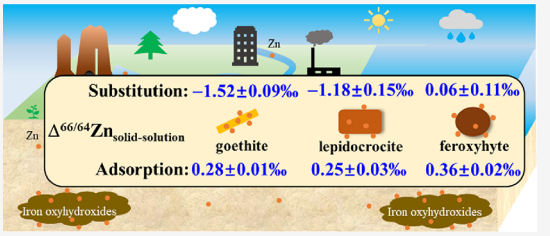

KEYWORDS: *metal (hydr)oxides, metal isotope fractionation, interface reactions, isomorphous substitution, adsorption, X-ray absorption fine-structure spectroscopy*

1. INTRODUCTION

Though an essential micronutrient at low concentrations, zinc (Zn) is toxic at high concentrations.[1] In terrestrial environments, high concentrations of Zn mainly result from intensive anthropogenic activities, including those associated with mining, smelting, chemical industries, agriculture, scrap disposal, combustion of domestic wastes, and processing of domestic waste waters as well as runoff from urban surfaces, but Zn also originates from natural sources, such as natural weathering and hydrothermal emissions.[2] As a result of these anthropogenic activities and natural processes, Zn-containing particles are released and subsequently weathered, and the release of dissolved Zn to soils as a result of weathering processes is probably the greatest source of Zn in the environment.[3] Once released and in order to better understand and predict Zn behavior, recent research is increasingly focused on the isotopic signatures associated with Zn biogeochemical cycling because these can fingerprint the different Zn sources, processes, and pathways that release Zn and control Zn mobility and fates.[4−8] The isotopic features of different Zn sources may be blurred however, by the biogeochemical processes and pathways that control its behavior, creating a "black box" of isotope signals that are extremely difficult to disentangle.[12] In particular, once Zn is released into the environment, Zn isotopes might be fractionated by a series of solid−solution interfacial reactions, such as adsorption, substitution and coprecipitation with minerals,[9−13] and mineral dissolution.[4,14−16] It is thus critical to investigate Zn isotope fractionation during these interfacial processes in order to use Zn isotopic signals to trace and track Zn in contaminated and natural systems.

In surficial environments, iron (Fe) (hydr)oxides play an important role in mediating the geochemical behavior and fate of metals in soils, sediments, and waters through adsorption and isomorphous substitution. While metal isotope fractionation during adsorption onto mineral surfaces is well-studied,[9,10,18−21] few studies have been conducted on fractionation during incorporation into Fe (hydr)oxide structures.[17] During adsorption processes, mineral crystalline structure, distribution of charge within the crystal lattices, presence of organic or mineral coatings, and solution chemistry

Received: October 29, 2022
Revised: March 30, 2023
Accepted: March 31, 2023
Published: April 12, 2023

may govern metal binding mechanisms and thus metal isotope fractionation direction and magnitude.[19,22] Previous work has reported that heavy Zn isotopes are preferentially adsorbed onto Fe (hydr)oxides with the fractionation magnitude for goethite much smaller than that for ferrihydrite.[19] Other studies however observed negative Zn isotope fractionations induced by adsorption onto Fe (hydr)oxides in acidic conditions.[18,23,24] During Zn adsorption onto quartz and amorphous silica, the fractionation magnitude for the former is much smaller than that for the latter, probably due to the different surface structural characteristics (e.g., structural disorder).[25] These results suggest that there may be different Zn isotope fractionations during adsorption onto different FeOOH polymorphs, which yet remains to be investigated.

Metal isotope fractionation induced by incorporation into the mineral structures involves much complex mechanisms. This process is generally interpreted from a kinetic fractionation effect, in which light isotopes are preferentially incorporated into the mineral structure owing to faster diffusion rates than heavy isotopes.[26−28] Isotope fractionation can also be caused by preferential attachment of one specific metal species onto the host mineral primary nuclei growth sites after fast aqueous isotopic exchange.[29] Crystal nucleation and growth mechanisms can also be particularly important. Isotope fractionation of Cd during incorporation into goethite for example is probably related to the ferrihydrite dissolution−goethite recrystallization mechanism.[17] Last but not least, the host mineral crystallization rate may affect the fractionation magnitude.[26,28,30] Despite the role that incorporation into Fe (hydr)oxides plays in controlling Zn mobility and fate, the isotope fractionation of Zn during this process and the mechanism(s) responsible for governing Zn isotope behavior are unknown.

Here, we aim to determine Zn isotope fractionation mechanisms during incorporation and adsorption with FeOOH polymorphs, including goethite (Goe), lepidocrocite (Lep), and feroxyhyte (Fero). The different structures of these FeOOH polymorphs may mean different crystal nucleation and growth mechanisms, metal uptake amounts,[31] and metal binding mechanisms.[32] It is therefore possible that incorporation and adsorption of Zn with these FeOOH polymorphs may induce different isotope fractionations. Zn K-edge X-ray absorption fine-structure spectroscopy (XAFS) and spherical aberration-corrected scanning transmission electron microscopy are used to determine Zn binding mechanisms in substituted and adsorbed Fe (hydr)oxide minerals. The mineral crystal nucleation and growth mechanisms, crystallization rates, and Zn binding mechanisms are then coupled to the Zn isotope fractionation during incorporation in and adsorption on these FeOOH polymorph minerals.

2. MATERIALS AND METHODS

All reagents were used as received without further purification and detailed information is presented in Text S1. The $ZnCl_2$ (≥98.0%, Sinopharm Chemical Reagent Co., Ltd., China) used in Zn-substituted FeOOH polymorph synthesis had a Zn isotope composition ($\delta^{66/64}$Zn) of −0.21 ± 0.05‰, while that of the 1000 mg·L^{-1} $Zn(NO_3)_2$ bulk solution (Guobiao Testing & Certification Co., Ltd., China) used in Zn adsorption experiments was −2.40 ± 0.05‰.

2.1. Preparation of Zn-Substituted FeOOH Polymorphs. Zinc-substituted FeOOH polymorphs with an initial Zn/Fe molar ratio of 0.02 were synthesized according to our previous study.[31] For Zn-substituted goethite (Goe), first, 90 mL of 5 M NaOH solution was added to 50 mL of 1 M $FeCl_3·6H_2O$ and a 20 mM $ZnCl_2$ mixture in an acid-cleaned 1 L Teflon bottle. Subsequently, the obtained suspension was diluted to 1 L with ultrapure water (18.2 MΩ·cm) under stirring until the pH was adjusted to >13 and aged for 60 h at 70 °C. For Zn-substituted lepidocrocite (Lep), 16 g of $FeCl_2·4H_2O$, 22.4 g of $(CH_2)_6N_4$, 5.6 g of $NaNO_2$, and 0.22 g of $ZnCl_2$ solids were added to 560 mL of ultrapure water in an acid-cleaned 1 L Teflon bottle (the pH of the suspension was ∼6.2) and then put in a water bath kettle under stirring at 60 °C for 3 h. For Zn-substituted feroxyhyte (Fero), 5 M NaOH solution was added to 300 mL of 0.1 M $FeCl_2·4H_2O$ and a 2 mM $ZnCl_2$ mixture to adjust the suspension pH to 8 under vigorous stirring in an acid-cleaned 1 L Teflon bottle, and then 30% H_2O_2 was added to the solution. The obtained green suspension gradually transformed into a reddish brown precipitate, and no further bubbles formed after ∼1 h.

At the end of each synthesis, 50 mL of suspension was withdrawn under vigorous stirring, and the solid and solution were separated by centrifugation. The solution was kept for further analysis and labeled as "supernatant" in order to differentiate it from that obtained during Zn adsorption experiments. The obtained solids (named as Zn2Goe, Zn2Lep, and Zn2Fero) were treated with 50 mL of 2 M HNO_3 solution for 0.5 h to remove adsorbed Zn species on the mineral surfaces (this part of Zn was labeled as "Adsorbed").[33] The remaining solids were named as Zn2Goe_n, Zn2Lep_n, and Zn2Fero_n.

In order to monitor the crystal formation processes, independent synthetic experiments were conducted. 25 mL of suspension was withdrawn at predetermined time intervals after heating of the initial reactant mixtures during the Zn-substituted Goe and Lep synthesis or upon the addition of H_2O_2 into the initial reactants during Zn-substituted Fero synthesis. The final pH values of the suspensions were 12.65 ± 0.05, 5.32 ± 0.05, and 2.22 ± 0.05. The suspensions were immediately centrifuged, and the as-obtained solids were thoroughly washed and then freeze-dried for further use.

2.2. Sample Characterization. Pure Goe, Lep, and Fero samples were synthesized as described above without the addition of Zn. The purity of the obtained solid samples was confirmed by powder X-ray diffraction (XRD) analysis (Figure S1). Quantitative phase analysis or Rietveld structure refinement of the intermediate solids during the synthesis of Zn-doped FeOOH polymorphs was conducted using TOPAS software version 4.2 (Bruker-AXS).[17] The specific surface areas of Goe, Lep, and Fero were determined to be 46, 168, and 116 $m^2·g^{-1}$ by multipoint BET modeling of the N_2 physical adsorption data, while the points of zero charge (PZCs) of these samples were measured to be ∼9.7, ∼8.5, and ∼ 9.4, respectively, by adopting a zeta potential method[17] (Figure S2). The sample morphologies were probed by electron microscopy (JEM-2010 HT, Japan) (Figure S3). The atomic images of Zn2Goe_n and Zn2Lep_n were obtained on a JEM-NEOARM spherical aberration-corrected scanning transmission electron microscopy at 200 kV (JEOL, Japan). Energy-dispersive X-ray spectroscope (EDS) quantitative analysis of single crystals for each mineral was also conducted.

The Fe and Zn concentrations in the solutions and solids were measured by flame atomic adsorption spectrometry (FAAS, Agilent Technologies 200 series AA) or inductively coupled plasma-optical emission spectrometry (ICP-OES,

https://doi.org/10.1021/acs.est.2c08028
Environ. Sci. Technol. 2023, 57, 6636−6646

Agilent 5110). The limit of detection for Zn by FAAS is 4.76 $\mu g \cdot L^{-1}$ with an uncertainty of 0.4%, while for ICP-OES, it is 9 $\mu g \cdot L^{-1}$ with an uncertainty of 2.0%.

2.3. Adsorption Experiments. The minerals were hydrated in 0.05 M KNO_3 solution for 24 h before Zn addition. For kinetic adsorption experiments, 91.7 or 152.9 μM Zn was reacted with 1 $g \cdot L^{-1}$ Goe or 0.5 $g \cdot L^{-1}$ Lep and Fero at pH 7 ± 0.05 for 48 h, during which suspension aliquots were withdrawn at predetermined intervals. Adsorption edge experiments were conducted between pH 4.0−8.0. Adsorption isotherms were conducted with Zn initial concentrations of 0−305.8 μM for Goe or 0−611.5 μM for Lep and Fero at pH 7 ± 0.05. The initial Zn concentrations were designed to obtain similar Zn coverages on these solids and to prevent Zn precipitation. The suspension pH was maintained by the addition of 1 M HNO3 or KOH solution. All adsorption experiments were conducted in Teflon tubes. A reaction time of 24 h was adopted by assuming that both adsorption and isotope fractionation equilibrium are approached according to literature.[19,34]

At the end of experiments, solids and supernatants were separated through 0.2 μm cellulose membranes. To remove dissolved Zn, the solids were immediately washed with background electrolyte and sequentially ultrapure water, the pHs of which were adjusted to be consistent with the adsorption experiments.[19] The washed solids were collected with membranes, sealed with Kapton tape, and then stored at 4 °C within 24 h for further Zn K-edge XAFS analysis. The Zn concentrations in the supernatants and solids after digestion were measured by FAAS. The obtained Zn-loaded solids were labeled as Zn*m*Goe_pH*n*, Zn*m*Lep_pH*n*, and Zn*m*Fero_pH*n*, in which *m* is the initial Zn concentration in $mg \cdot L^{-1}$ and *n* is the reaction pH. Replicated experiments were carried out 2−3 times to ensure reproducibility.

A Zn adsorbed ferrihydrite (Fh) standard, Zn20Fh_pH7.5, was also prepared by reacting 0.31 mM Zn with 0.5 $g \cdot L^{-1}$ Fh (synthesized according to a previous study)[17] for 24 h at pH 7 ± 0.05 in 0.05 M KNO_3 solution.

2.4. Purification and Measurement of Zn Isotopes by MC-ICP-MS. Zinc-containing solids were digested using 12 M HCl and 15 M HNO_3 solutions until dry and then redissolved in 2 M HCl solution. About 3 μg of Zn was weighed for Zn purification. After drying, 2 mL of 2 M HCl was added, and the solution was transferred into a 15 mL polypropylene centrifuge tube. Samples were then purified on columns containing 3 mL of pre-cleaned 100−200 mesh AG MP-1M (Bio-Rad, USA) anion-exchange resin.[35,36] After the adsorption of metals onto the column, 30 mL of 2 M HCl and 12 mL of 0.3 M HCl were passed through the columns, respectively. Zn was eluted using 12 mL of 0.012 M HCl. The solution was evaporated to dryness at 110 °C and dissolved in 3 mL of 1% HNO_3. Additionally, 0.5 mL of the final solution was used for Zn measurement to monitor the recovery, and the residue was used for Zn isotope analysis. Satisfactory recoveries were obtained for the unprocessed and processed samples (>98%).

Zinc isotope ratios were measured using a Thermo Scientific Neptune plus MC-ICP-MS at the State Key Laboratory of Crust−Mantle Evolution and Mineralization at Nanjing University. Instrumental mass bias was corrected using a coupled method of sample-standard bracketing (SSB) and Cu doping. More details are provided in Text S2. Sample Zn isotope ratios were reported in standard delta notation in per mil units relative to IRMM 3702 Zn solution according to eq 1:

$$\delta^{66/64}\mathrm{Zn} = \left[\frac{(^{66}\mathrm{Zn}/^{64}\mathrm{Zn})_{\mathrm{sample}}}{(^{66}\mathrm{Zn}/^{64}\mathrm{Zn})_{\mathrm{std}}} - 1\right] \times 1000 \quad (1)$$

Since a mass-dependent fractionation law applies to all samples (Figure S4), only $\delta^{66/64}$Zn was reported. CAGS-1 and the new AA-ETH Zn isotope standard solutions were used as internal laboratory secondary reference materials, and the $\delta^{66/64}Zn_{\mathrm{IRMM\ 3702}}$ values were −0.85 ± 0.05‰ (n = 6) and −0.01 ± 0.05‰ (n = 6), respectively, agreeing well with previously reported values.[35,37] An in-house sulfide standard (BCR-2) was used to monitor potential Zn isotope fractionation during purification, and the analyses of BCR-2 yielded $\delta^{66/64}Zn_{\mathrm{JMC\text{-}Lyon}}$ of 0.28 ± 0.02‰ (n = 2), consistent with reported values.[38] The long-term reproducibility of 0.05‰ was used for data measured with 2SD value of <0.05‰. The Zn isotope fractionation ($\Delta^{66/64}Zn_{\mathrm{solid\text{-}solution}}$) between solid and aqueous phases is defined as eq 2:

$$\Delta^{66/64}\mathrm{Zn}_{\mathrm{solid-solution}} = \delta^{66/64}\mathrm{Zn}_{\mathrm{solid}} - \delta^{66/64}\mathrm{Zn}_{\mathrm{solution}} \quad (2)$$

2.5. Zn K-Edge XAFS Data Collection and Analysis. Zinc K-edge XAFS spectra for Zn-containing samples along with aqueous Zn(NO3)2 were collected on beamline 1W2B at BSRF at room temperature with a pair of Si(111) monochromators in fluorescence or transmission mode. The Zn metal foil (E_0 = 9659 eV) was used for energy calibration. The data processing and analysis were performed using the IFEFFIT software.[39] The parameters used for background removal were as follows: E_0 = 9667 eV, k-weight = 2, and R_{bkg} = 1.1. Structural parameters (R, CN, and σ^2) were obtained by fitting the experimental k^2-weighted data to the standard equation.[40] An amplitude reduction factor (S_0^2) of 0.85 was used.[20]

3. RESULTS AND DISCUSSION

3.1. Zn Isotope Fractionation during Adsorption on FeOOH Polymorphs. Similar Zn adsorption kinetics, pH adsorption edges, and adsorption isotherms are observed for these FeOOH polymorphs (Figure S5 and Table S1). The maximum Zn adsorption densities on Goe, Lep, and Fero obtained by Langmuir fitting are 2.47, 2.62, and 4.12 $\mu mol \cdot m^{-2}$, respectively (Table S2).

Analysis of the isotopic compositions of the solutions and solids shows that heavy Zn isotopes are preferentially enriched on the mineral surfaces. As the reaction pH raises from 6 to 8, the proportion of Zn adsorbed (f) increases from 19.0 to 91.4% for Goe, from 18.1 to 92.7% for Lep, and from 20.6 to 96.8% for Fero, while correspondingly, the $\delta^{66/64}Zn_{\mathrm{solution}}$ value decreases from −2.42 ± 0.05‰ to −2.62 ± 0.05‰, from −2.50 ± 0.05‰ to −2.77 ± 0.05‰, and from −2.40 ± 0.08‰ to −2.61 ± 0.05‰ (Table S3), respectively. When the isotopic compositions are plotted as a function of f (Figure 1), it is clear that experimental $\delta^{66/64}$Zn values in the solutions and solids linearly decrease as f increases. The data are fitted with both an equilibrium (eq 3) and Rayleigh model (eq 4):

$$\delta^{66/64}\mathrm{Zn}_{\mathrm{solution}} = \frac{\delta^{66/64}\mathrm{Zn}_{\mathrm{stock\ solution}} - 1000 \cdot f(\alpha_{\mathrm{solid-solution}} - 1)}{1 + f(\alpha_{\mathrm{solid-solution}} - 1)} \quad (3)$$

https://doi.org/10.1021/acs.est.2c08028
Environ. Sci. Technol. 2023, 57, 6636−6646

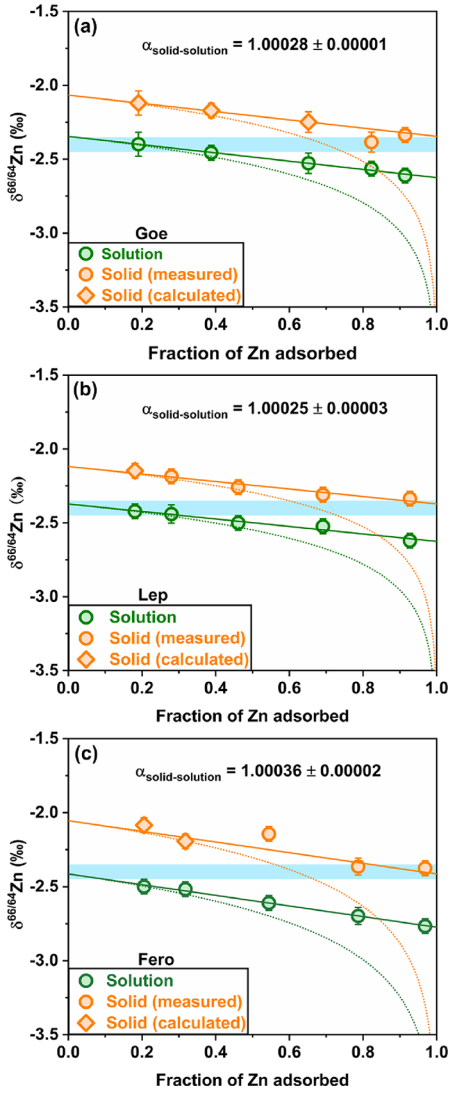

Figure 1. Zn isotopic compositions of solution and solid phases as a function of adsorbed Zn fraction (f) during adsorption onto Goe (a), Lep (b), and Fero (c). The lines and dashed curves represent the theoretical $\delta^{66/64}$Zn values calculated using the equilibrium model and the Rayleigh model, respectively. Several $\delta^{66/64}$Zn values of the solids (diamonds) were calculated according to the mass balance $\delta^{66/64}Zn_{solid} = (\delta^{66/64}Zn_{stock\ solution} - \delta^{66/64}Zn_{solution} \times (1 - f))/f$. The $\delta^{66/64}$Zn of the bulk Zn solution used for adsorption experiments is −2.40 ± 0.05‰.

$$\delta^{66/64}Zn_{solution} = (1000 + \delta^{66/64}Zn_{stock\ solution}) \cdot (1 - f)^{(\alpha_{solid-solution}-1)} - 1000 \quad (4)$$

where $\alpha_{solid\text{-}solution}$ represents the estimated isotope fractionation factor between adsorbed and aqueous Zn and $\delta^{66/64}Zn_{stock\ solution}$ denotes the estimated value for stock solution. The equilibrium model applies to systems in which forward and backward reactions occur at similar rates, while the Rayleigh model applies to homogeneous reactant pools where light isotopes are continuously and preferentially removed.[41]

The fits generated using the equilibrium model agree much better with the experimental data than those using the Rayleigh model. This demonstrates that Zn isotope fractionation during adsorption onto the FeOOH polymorphs results from an equilibrium fractionation mechanism. The derived fractionation factors ($\alpha_{solid\text{-}solution}$) are 1.00028 ± 0.00001, 1.00025 ± 0.00003, and 1.00036 ± 0.00002 for Goe, Lep, and Fero, respectively. The isotope fractionation between adsorbed and dissolved Zn can be calculated according to the isotope fractionation factor (eq 5):

$$\Delta^{66/64}Zn_{solid-solution} \cong 1000 \times \ln \alpha_{solid-solution} \quad (5)$$

The $\Delta^{66/64}Zn_{solid\text{-}solution}$ are thus calculated to be 0.28 ± 0.01‰, 0.25 ± 0.03‰, and 0.36 ± 0.02‰ for Goe, Lep, and Fero, respectively. This suggests that Zn adsorption on these three FeOOH polymorphs induces a similar isotope fractionation.

3.2. Zinc Binding Environments in the Zn-Containing Samples. Both Zn K-edge X-ray absorption near edge structure (XANES) and extended X-ray absorption fine structure (EXAFS) spectra were used to analyze the Zn binding mechanisms in typical Zn-containing samples. XANES spectra of all samples display broadening and/or splitting of the main edge at ∼9672 eV (Figure 2A), due to the contribution of second Fe neighbors.[42] A well-defined peak at ∼9688 eV is observed for aqueous $Zn(NO_3)_2$ and Zn-substituted samples Zn2Goe_n and Zn2Lep_n, suggesting that Zn is predominantly in an octahedral (^{VI}Zn) geometry in the substituted samples and predominantly tetrahedral (^{IV}Zn) complexes in the adsorbed samples.[24,42−44] Linear combination fitting of the adsorbed samples using Zn20Fh_pH7.5 and Zn2Goe_n as endmembers, in which exclusively ^{IV}Zn or ^{VI}Zn exists, respectively,[19,44−46] demonstrates that Zn-adsorbed Fero samples contain only ^{IV}Zn, Zn-adsorbed Lep samples contain 17−27% ^{VI}Zn, while Zn-adsorbed Goe samples contain 31−40% ^{VI}Zn (Table S4). Previous studies have demonstrated that Zn is adsorbed on goethite as octahedral[19] but also tetrahedral complexes.[23,47] The varying proportions of ^{IV}Zn and ^{VI}Zn may be related to the mineral characteristics and solution chemistry.

In the k^2-weighted EXAFS spectra (Figure 2B), there is a shift in the first oscillation of the Zn adsorbed samples to high k (∼4.0 Å^{-1}) relative to that of the aqueous $Zn(NO_3)_2$ and Zn-substituted samples (∼3.7 Å^{-1}). This shift indicates a change of Zn−O first shell coordination from octahedral to tetrahedral,[48] further confirming the XANES analysis. In the Fourier transformed spectra (Figure 2C), the obvious peaks beyond the first Zn−O shell indicate the formation of Zn inner-sphere complexes on the mineral surfaces or incorporation into the lattices. Shell-by-shell EXAFS fitting (Table S4) shows an average Zn−O distance of 2.07 ± 0.01 Å for aqueous $Zn(NO_3)_2$ and of 1.99 ± 0.01 Å for ^{IV}Zn in Zn adsorbed ferrihydrite, which agree well with the previous literature.[9,19,47,49] Similar average Zn−O distances of 1.98−1.99 Å are observed for the Zn-adsorbed samples. These distances are closer to those for tetrahedral Zn. This is consistent with the linear combination fitting, which shows that Zn adsorbed on Fero, Lep, and Goe is predominantly tetrahedral but with an increasing amount of octahedral Zn, respectively (Table S4). Similar results were previously observed for Zn−O distances in hydrozincite (∼2.00 Å),[9] Zn adsorbed on manganite (1.98−2.04 Å)[50] and on todorokite at pH 6−8 (2.00−2.05 Å).[9] Two Zn−Fe distances of 3.12−3.25 and 3.35−3.49 Å are also observed for Zn-adsorbed Fh, Fero, and Goe. This indicates the formation of bidentate edge- and corner-sharing complexes on the mineral surfaces (Figure 2D,F).[43,19,49] In contrast, only a Zn−Fe distance of 3.11−3.13 Å is detected for Zn-adsorbed

https://doi.org/10.1021/acs.est.2c08028
Environ. Sci. Technol. 2023, 57, 6636−6646

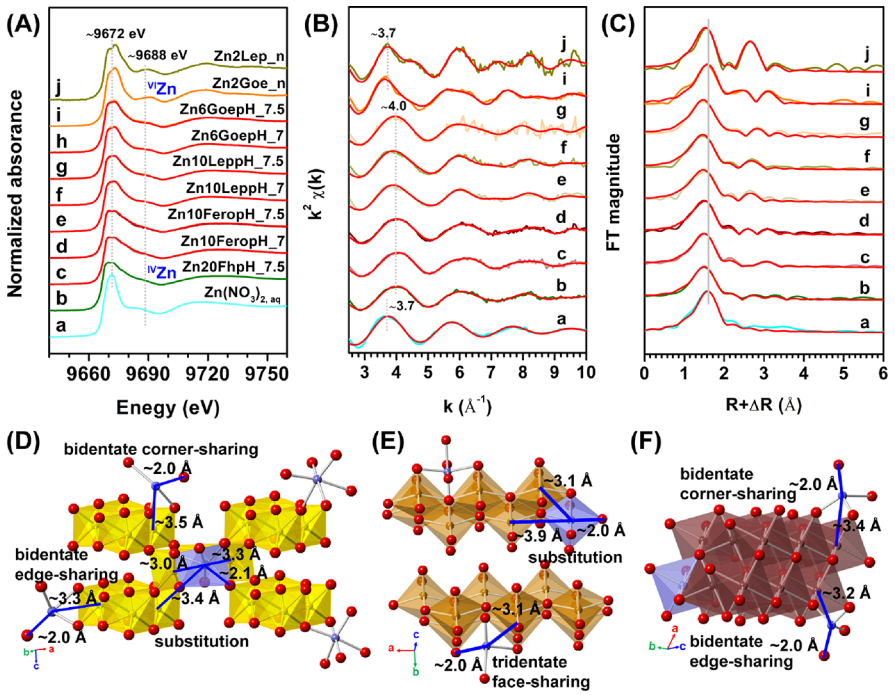

Figure 2. Zinc K-edge XANES (A), k^2-weighted EXAFS (B), and the corresponding Fourier transformed spectra (FTs, C) of typical Zn adsorbed, substituted samples, and aqueous $Zn(NO_3)_2$ standard ($Zn(NO_3)_{2,aq}$), overlaid with the best fits. The experimental data are displayed as colored lines and the best fits are shown as red lines. The adsorbed samples were named as Zn*m*Goe_pH*n*, Zn*m*Lep_pH*n*, and Zn*m*Fero_pH*n*, in which *m* is the initial Zn concentration in mg·L^{-1} and *n* is the reaction pH. The Zn-substituted samples were labeled as Zn*m*Goe_*n* and Zn*m*Lep_*n*, in which m is the initial Zn/Fe molar ratio. During linear combination fitting of the Zn K-edge XANES spectra for the Zn adsorbed samples, Zn-adsorbed ferrihydrite sample (Zn20Fh_pH7.5) and Zn-substituted goethite sample (Zn2Goe_n) were used as tetrahedral (^{IV}Zn) and octahedral (^{VI}Zn) endmembers. A schema representing the local environments of Zn adsorbed onto and incorporated into goethite (D), lepidocrocite (E), and feroxyhyte (F).

Lep, which can be assigned to tridentate face-sharing complexes (Figure 2E).[19] For Zn-substituted Goe, an average Zn−O distance of 2.07 ± 0.01 Å and three Zn−Fe distances at 3.02 ± 0.03, 3.33 ± 0.06, and 3.49 ± 0.05 Å are observed. These distances correspond well to those observed for Zn-substituted goethite.[51] For Zn-doped Lep, a Zn−O distance of 2.01 ± 0.01 Å and two Zn−Fe distances of 3.11 ± 0.02 and 3.90 ± 0.08 Å support the incorporation of Zn into the mineral lattices according to the mineral crystal structure.

3.3. Isotope Fractionation Mechanisms during Zn Adsorption on FeOOH Polymorphs. Our results clearly suggest that heavy Zn isotopes are preferentially partitioned onto the FeOOH mineral surfaces, which is in good agreement with previous studies.[10,19,20,25] It was previously reported that heavy Zn isotopes are enriched on Fe, Si, Al, and Mn (hydr)oxides surfaces during adsorption processes owing to the formation of inner-sphere complexes with shorter Zn−O lengths compared to aqueous Zn.[19,20,25,52,53] Generally, heavier metal isotopes are preferentially concentrated in stiffer bonding environments, e.g., coordinated to highly covalent bonds, with lower coordination number and shorter bond lengths.[12,41] The Zn K-edge XAFS analysis shows that Zn adsorbed onto Goe, Lep, and Fero form inner-sphere complexes with Zn−O bond lengths ranging from 1.98−1.99 Å that are much shorter than that of octahedral Zn in solution (2.07 ± 0.01 Å) (Table S4). These bond length differences are probably responsible for adsorption-induced enrichment of heavy Zn isotopes onto these FeOOH polymorphs. The fact that these Zn−O bond lengths are almost the same for the different FeOOH polymorphs (Table S4) also explains why we observe a similar $\Delta^{66/64}Zn_{solid\text{-}solution}$ of 0.25−0.36‰ for Goe, Lep, and Fero. Though Zn K-edge XANES linear combination fitting shows that Zn is predominantly adsorbed as ^{IV}Zn on Fero, Lep, and Goe but with increasing proportions of ^{VI}Zn in the latter two, EXAFS analysis, which fits the average bonding environment, gives essentially the same Zn−O distances. As such, our results indicate that having only ^{IV}Zn (feroxyhyte) or a mixture of ^{IV}Zn−^{VI}Zn (goethite/lepidocrocite) does not significantly modify the recorded $\Delta^{66/64}Zn_{solid\text{-}solution}$ (difference < 0.1‰), which may be ascribed to the weaker effect of ^{VI}Zn than ^{IV}Zn on isotope fractionation magnitude during adsorption on Fe (hydr)oxides.[44]

It is noteworthy that although our study confirms the enrichment of heavy Zn isotopes during adsorption on Fe (hydr)oxides as revealed by some previous studies,[19] others observed negative $\Delta^{66/64}Zn_{solid\text{-}solution}$ during Zn adsorption on goethite in acid conditions (e.g., pH 5.3−6.1).[18,23,24] In contrast, positive $\Delta^{66/64}Zn_{solid\text{-}solution}$ is observed at higher pHs (6−8) here and in a previous study.[19] We therefore hypothesize that pH and Zn solution speciation may play important roles in Zn isotope fractionation direction and magnitude.[18,23] For example, relative to $Zn(H_2O)_6^{2+}$, Zn-$(OH)(H_2O)_5^{+}$ and $Zn(OH)_2(H_2O)_4$, the proportions of which are increased at higher pH, enrich relatively heavy isotopes.[54] Speciation calculations in the current study however show that aqueous $Zn(H_2O)_6^{2+}$ is the dominant species (~95%) with only limited $ZnNO_3(H_2O)_5^{+}$ (5%) over pH 4−8 (Figure S6). This suggests that Zn aqueous speciation contributes little to the Zn isotope fractionation during adsorption onto the FeOOH polymorphs in the present study. Thus, it is possible

https://doi.org/10.1021/acs.est.2c08028
Environ. Sci. Technol. 2023, 57, 6636−6646

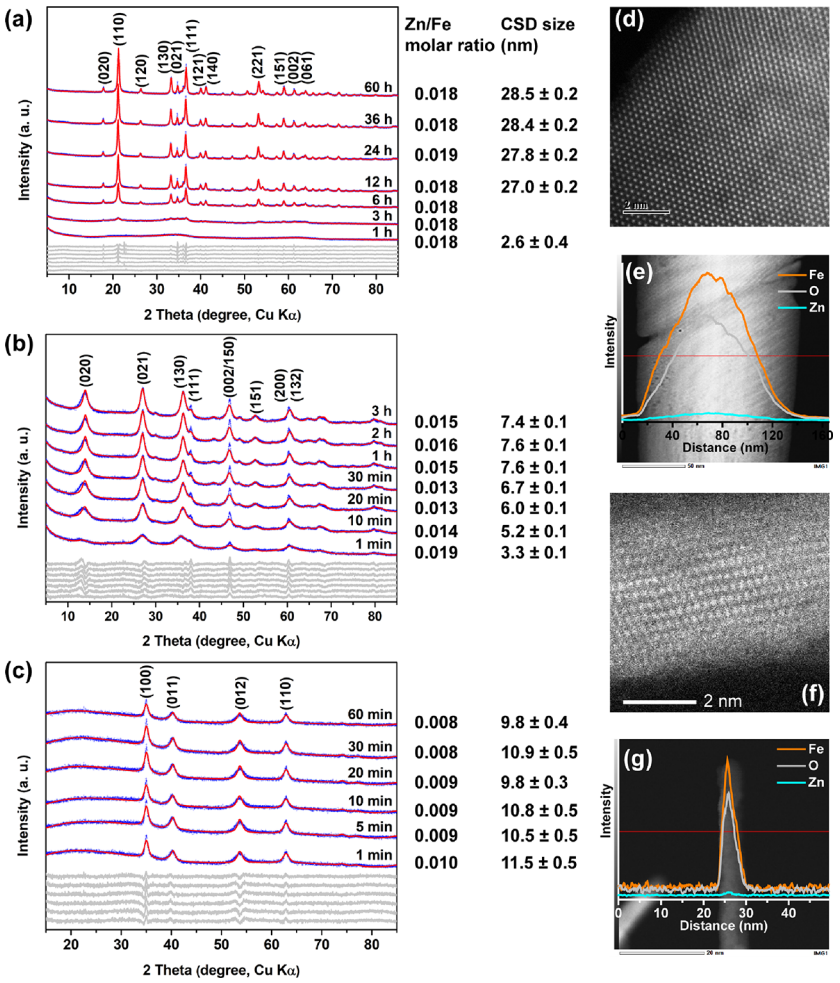

Figure 3. Powder XRD patterns, final Zn/Fe molar ratios and coherent scattering domain (CSD) sizes of the reaction intermediates during the synthesis of Zn-substituted goethite (a), lepidocrocite (b), and feroxyhyte (c). The XRD experimental patterns (blue crosses) are overlaid with the best Rietveld structure refinement or quantitative phases analysis results (red lines), based on the structure models of goethite (ICSD 71810), ferrihydrite (ICSD 158475), lepidocrocite (ICSD 108876), and feroxyhyte (ICSD 291515). The difference patterns are shown as gray lines at the bottom. All experiments were conducted at an initial Zn/Fe molar ratio of 0.02. Atomic resolution images and EDS line scans of Zn-substituted goethite sample, Zn2Goe_*n* (d and f), and Zn-substituted lepidocrocite sample, Zn2Lep_*n* (e and g).

that different isotope fractionation mechanisms dominate at low and high pH conditions during Zn adsorption onto goethite but confirmation of this requires further study.

3.4. Crystal Formation Processes of Zn-Substituted FeOOH Polymorphs. In order to better understand the Zn isotope fractionation during substitution into the FeOOH polymorph minerals, we first discuss the crystal growth processes. Powder XRD analysis of intermediate solids during Zn-substituted Goe synthesis shows the formation of goethite (ICSD 71870) via a ferrihydrite precursor (ICSD 158475) (Figure 3a and Figure S7a).[17,27,55] Specifically, the diffraction peaks of goethite appear within 3 h and then gradually increase with time and stay almost unchanged after 12 h. The ferrihydrite formed at 1 h has a coherent scattering domain (CSD) size of 2.6 ± 0.4 nm (Figure 3a, Table S5). Quantitative phase analysis of the 3 and 6 h solids shows 61 ± 10% and 13 ± 5% ferrihydrite, and the precursor is almost completely transformed to goethite at 12 h. The average CSD sizes of the goethite particles slightly increase from 27.0 ± 0.2 nm at 12 h to 28.5 ± 0.2 nm at 60 h. Owing to the high reaction pH (~12.7) and the reactivity of ferrihydrite/goethite toward metals, almost all the initial Zn is retained on the intermediate solids with constant Zn/Fe molar ratios of 1.8−1.9%.

Unlike the Zn-doped Goe system, there is probably no ferrihydrite precursor during the Zn-doped Lep synthesis under the current experimental conditions (pH ~ 5.3). XRD patterns show the appearance of weak crystalline lepidocrocite (ICSD 108876) after reaction for 1 min but without ferrihydrite (Figure 3b and Figure S7b). This is consistent with previous studies showing that lepidocrocite dominates upon Fe^{2+} oxidation at pH > 5 while ferrihydrite dominates at pH < 5.[56] As the reaction progresses, a gradual increase in the XRD peak intensity indicates increasing mineral crystallinity within 1 h. The particle CSD size increases from 3.3 ± 0.1 nm at 1 min to 7.6 ± 0.1 nm at 1 h and then remains constant (Table S5). This may indicate that Lep is formed through a direct nucleation and crystal growth mechanism. Concurrently, owing to the finite particle size, at 1 min, the solid has a Zn/Fe ratio of 1.9 ± 0.0%. As the crystal grows and particle size increases, some of the Zn may be released back into solution and at 30 min, the solid Zn/Fe ratio decreases to 1.3%. The solids from 1−3 h have Zn/Fe ratios of 1.5−1.6%, probably owing to Zn re-adsorption onto the solid.

https://doi.org/10.1021/acs.est.2c08028
Environ. Sci. Technol. 2023, 57, 6636−6646

Similar to that of Zn-doped Lep formation, the Fero crystal (ICSD 291515) is directly formed by Fe^{2+} oxidation without ferrihydrite formation (Figure 3c and Figure S7c).[56] The Fero crystal nucleation and growth however occur at much higher rates than those of Lep, e.g., for the Fero crystal, nucleation and growth are almost complete in the first minute, as evidenced by the almost unchanged XRD peak intensities and CSD sizes of the intermediate solids (9.8−11.5 nm) as the reaction goes on (Table S5). The Zn/Fe molar ratios in these intermediates slightly decrease from 1.0 ± 0.0% in the 1 min solid to 0.8 ± 0.0% in the 60 min solid, probably owing to the competition by protons for active sites at a pH of ∼2.2.

The final molar ratios of Zn/Fe in Zn2Goe_*n*, Zn2Lep_*n*, and Zn2Fero_*n* are 1.9 ± 0.0%, 1.3 ± 0.0%, and 0.4 ± 0.0%, respectively. Zn cations removed by HNO_3 treatment of Zn2Goe, Zn2Lep, and Zn2Fero samples are probably those adsorbed on these mineral surfaces. This can be confirmed by several lines of evidence. First, only 2.0%, 7.2%, and 7.3% of the total Fe are removed from these samples (Figure S8). Second, powder XRD patterns of these samples before and after HNO_3 treatment are almost the same (Figure S9). Thus, the solids obtained after HNO_3 treatment are Zn-substituted minerals. Atomic images of Zn2Goe_*n* and Zn2Lep_*n* show the uniform distribution of Zn in the crystal lattices (Figure 3d,f). This is further confirmed by the EDS line scan of single crystals for each mineral that clearly shows the strong correlations between Fe, Zn, and O (Figure 3e,g). Furthermore, the EDS analysis gives an average Zn/Fe molar ratio of 2.1 ± 0.1% for Zn2Goe_*n* and 1.0 ± 0.1% for Zn2Lep_*n* (Figure S10), which agree well with the wet chemical analysis results.

3.5. Zn Isotope Fractionation during Substitution for Fe in FeOOH Polymorphs. At the end of Zn2Goe synthesis, Zn isotope compositions in the supernatant ($\delta^{66/64}Zn_{supernatant}$) and in the solid ($\delta^{66/64}Zn_{Zn2Goe}$) are 1.27 ± 0.05‰ and −0.15 ± 0.07‰, respectively (Figure 4 and Figure S8). The latter is identical to the Zn stock solution (−0.21 ± 0.05‰) due to the fact that almost all Zn is retained in Zn2Goe. After 2 M HNO_3 treatment, $\delta^{66/64}Zn$ for Zn incorporated into goethite ($\delta^{66/64}Zn_{Zn2Goe\_n}$) is −0.16 ± 0.05‰, while $\delta^{66/64}Zn$ for Zn in HNO_3 solution ($\delta^{66/64}Zn_{Adsorbed}$) is −0.07 ± 0.05‰ (Figure 4 and Figure S8). The $\delta^{66/64}Zn$ of Zn2Lep and the corresponding supernatant are −0.28 ± 0.08‰ and 0.40 ± 0.05‰, while $\delta^{66/64}Zn_{Zn2Lep\_n}$ and $\delta^{66/64}Zn_{Adsorbed}$ decrease to −0.45 ± 0.05‰ and 0.12 ± 0.08‰, respectively. In contrast, $\delta^{66/64}Zn$ of Zn2Fero and the corresponding supernatant are −0.09 ± 0.05‰ and −0.25 ± 0.05‰, respectively, while $\delta^{66/64}Zn_{Zn2Fero\_n}$ decreases to −0.24 ± 0.05‰ and $\delta^{66/64}Zn_{Adsorbed}$ increases to 0.18 ± 0.05‰.

According to the isotope signals of different Zn pools during these processes, we can also calculate the Zn isotope compositions ($\delta^{66/64}Zn_{substituted}$) of the Zn-substituted FeOOH polymorph minerals (eq 6).

$$\delta^{66/64}Zn_{stock\ solution} = f_1 \times \delta^{66/64}Zn_{supernatant} + f_2 \times \delta^{66/64}Zn_{adsorbed} + f_3 \times \delta^{66/64}Zn_{substituted} \quad (6)$$

where f_1, f_2, and f_3 refer to the fractions of Zn in supernatant, adsorbed on the mineral surfaces, and incorporated into the crystal lattices, respectively. Based on eq 6, the $\delta^{66/64}Zn_{substituted}$ values are calculated to be −0.22 ± 0.05‰, −0.46 ± 0.09‰, and −0.14 ± 0. 10‰ for Zn2Goe_*n*, Zn2Lep_*n*, and Zn2Fero_*n*, respectively, which are consistent with the measured values. In these systems, adsorption and substitution processes both lead to the distribution of Zn between solution and solid and thus isotope fractionation.

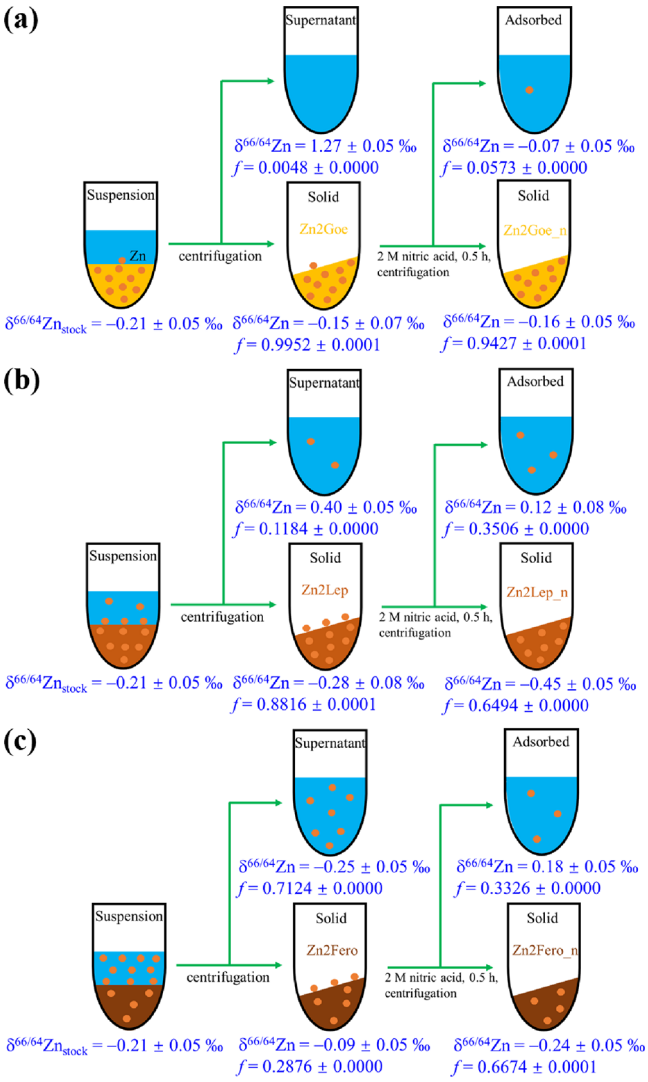

Figure 4. Schematic illustration of the experimental protocols for Zn isotope fractionation analysis during Zn substitution in (a) Goe, (b) Lep, and (c) Fero. The Zn isotope composition and the fraction of Zn (f) at each step were presented. The $\delta^{66/64}Zn$ of $ZnCl_2$ used for Zn-substituted FeOOH polymorphs synthesis is −0.21 ± 0.05‰. It should be noted that the different f cannot be summed to obtain 100% and each step considers a new total population (100%), which is divided into two parts.

If we assume that the two isotope fractionation factors involved here, for adsorption and incorporation, follow an equilibrium regime, the Zn isotope fractionation during incorporation into the lattices of these minerals ($\Delta^{66/64}Zn_{substituted\text{-}stock\ solution}$) can be calculated according to the isotope mass balance (eq 7):

$$\Delta^{66/64}Zn_{solid-supernatant} = f_2/(f_2 + f_3) \times \Delta^{66/64}Zn_{adsorbed-supernatant} + f_3/(f_2 + f_3) \times \Delta^{66/64}Zn_{substituted-stock\ solution} \quad (7)$$

https://doi.org/10.1021/acs.est.2c08028
Environ. Sci. Technol. 2023, 57, 6636−6646

where $\Delta^{66}Zn_{solid\text{-}supernatant}$ refers to Zn isotope fractionation between supernatant and solid at the end of the FeOOH formation and equals −1.42 ± 0.09‰, −0.68 ± 0.09‰, and 0.16 ± 0.07‰ for Zn2Geo, Zn2Lep, and Zn2Fero, respectively. Thus, the $\Delta^{66/64}Zn_{substituted\text{-}stock\ solution}$ values are calculated to be −1.52 ± 0.09‰, −1.18 ± 0.15‰, and 0.06 ± 0.11‰ for Zn2Goe_*n*, Zn2Lep_*n*, and Zn2Fero_*n*, respectively. These results clearly indicate that Zn substitution enriches light isotopes in goethite and lepidocrocite but almost no isotope fractionation occurs in feroxyhyte under the experimental conditions.

3.6. Zn Isotope Fractionation Mechanisms during Substitution for Fe in FeOOH Polymorphs. About >94% Zn is retained in the Zn2Goe_*n* solid by substituting for lattice Fe, and this results in a substantial negative isotope fractionation (−1.52 ± 0.09‰) (Figure 4a and Figure S8A). EXAFS analysis shows that Zn substitutes for lattice Fe in Zn2Geo_*n* with a Zn−O bond length the same as that (2.07 ± 0.01 Å) for aqueous Zn. This suggests that the enrichment of light Zn isotopes in Zn2Geo_*n* is not related to the Zn coordination environment but rather is probably related to the goethite formation process. Goethite generally forms from Fh dissolution−Goe recrystallization processes.[27,55] In tandem with the Fh formation, lighter Zn isotopes are preferentially incorporated in and/or adsorbed onto the solid due to a kinetic effect, in which lighter isotopes diffuse faster than heavier ones (e.g., within 1 h, Figure 3a). This results in the enrichment of heavy Zn isotopes in the solution with $\delta^{66/64}Zn_{supernatant}$ > 1.27 ± 0.05‰. Subsequently, Fh particles slowly dissolve, releasing into the solution soluble Fe as a nucleus to form the Goe and Zn species as suitable growth units (e.g., 1−12 h, Figure 3a). This process may also be kinetically controlled, such that isotopically light Zn is released into the surrounding solution. It was previously reported that in the early stages of proton- and oxalate-promoted dissolution of finely powdered biotite granite, isotopically light Zn was released following a kinetic isotope fractionation.[16] Further, the Zn released is expected to be relatively isotopically light because heavy Zn isotopes are preferentially adsorbed on/incorporated in the ferrihydrite by adopting a tetrahedral geometry.[49] Notwithstanding this, the released relatively light Zn isotopes are probably in tetrahedral coordination.[19,42,49] After their release, a transformation from tetrahedral to octahedral would occur and then the octahedral Zn is directly attached onto the goethite growth unit. Alternatively, the released Zn tetrahedra can be immediately attached onto the goethite growth unit and then transform to octahedra. Although all these kinetically controlled isotope fractionation processes that are possibly involved during Zn substitution in goethite can contribute to the enrichment of light Zn isotopes in the goethite lattices, kinetic effects often occur in the first few hours of metal−mineral interactions.[22] After this initial window, Zn adsorbed on the mineral surfaces and that remaining in the supernatant exchange and reach adsorption/desorption equilibrium and isotope fractionation equilibrium. Thus, the 1.27 ± 0.05‰ Zn isotope signal of the supernatant at the end of Zn-doped goethite synthesis is possibly the result of a complex series of kinetic and equilibrium processes. Further, the calculated large $\Delta^{66/64}Zn_{substituted\text{-}stock\ solution}$ (−1.52 ± 0.09‰) suggests that the isotope signal of Zn-substituted goethite is predominantly inherited from the Zn associated with the ferrihydrite precursor. The exact mechanisms of Zn isotope fractionation during incorporation into goethite however require further investigations at varying pH and Zn/Fe molar ratios.

A Zn isotope fractionation of −1.18 ± 0.15‰ is derived for Zn incorporation into the Lep structure and is probably also caused by a complex suite of mineral nucleation and growth processes (Figure 3b). At the initial stage (< 1 min), finite Lep particles directly nucleate from solution,[56] and almost all the Zn is retained on the solids (Figure 3b). As the Lep crystals grow larger with time (1−60 min), part of the Zn is incorporated into the lattices, while part of the Zn is released back into solution, especially in the first 9 mins. The Zn released is probably that previously adsorbed on the solid surfaces during 0−1 min and is probably relatively heavy according to the adsorption experiments. This decreases the solid $\delta^{66/64}$Zn. After crystal growth is complete at ∼1 h, Zn adsorption−desorption reactions dominate and probably approach equilibrium, and as-induced isotope exchanges occur simultaneously. During this stage, relatively heavy isotopes are adsorbed onto the Zn2Lep_*n* surfaces. This may consequently counteract the negative isotope fractionation during Zn incorporation into the lattices, resulting in the $\delta^{66/64}$Zn of Zn2Lep that is indistinguishable from that of the stock solution (Figure 4b and Figure S8B).

The $\delta^{66/64}$Zn value for Zn2Fero is higher than the stock solution (Figure 4c and Figure S8C), probably owing to the adsorption of heavy Zn isotopes onto the solids. Removal of the adsorbed Zn on the mineral surfaces by acid washing decreases the $\delta^{66/64}$Zn value of Zn2Fero_*n* so that it is indistinguishable from the stock solution. The negligible Zn isotope fractionation (0.06 ± 0.11‰) in Zn2Fero_*n* is probably closely related to the fast crystal nucleation and growth that is almost complete in 1 min (Figure 3c). This is consistent with previous studies showing that the expression of kinetic isotope effects should be prevented in the solids when produced at extremely rapid precipitation rates.[28] Later (1−60 min), relatively heavy Zn isotopes in the residual solution pool are specifically adsorbed onto the solid surfaces, while at the same time, protons strongly compete for adsorption sites and drive the release of relatively light Zn isotopes into solution.[16]

The different $\Delta^{66/64}Zn_{substituted\text{-}stock\ solution}$ induced by Zn substitution for lattice Fe in these FeOOH polymorphs may be strongly related to their different nucleation and growth rates, in addition to their different formation pathways. Several previous studies have examined the effects of precipitation rates on Fe isotope fractionation. In general, typically small or almost no Fe isotope fractionation is observed when precipitation occurs either very fast or very slowly (e.g., hundreds of days).[26,30] Significant isotope fractionations occur however when the precipitation progresses over time scales of hours to weeks.[26,28] In the present study, the time scales for Zn2Goe_*n* and Zn2Lep_*n* nucleation and growth range from 1 h to 12 h, while that for Zn2Fero_*n* is within 1 min (Figure 3). The calculated $\Delta^{66/64}Zn_{substituted\text{-}stock\ solution}$ values for these Zn substituted FeOOH polymorphs are also comparable to those for Fe(III) precipitated at similar precipitation rates.[26,30] As the initial crystal nucleation and growth rates for Zn2Goe_*n* and Zn2Lep_*n* are relatively low, diffusion gradient-controlled Zn incorporation into the growing solids results in the large negative isotope fractionations observed. However, for Zn2Fero_*n*, diffusion gradients in the liquid boundary layer around the primary feroxyhyte nuclei may limit isotope exchange between the residual Zn in this layer and the bulk

https://doi.org/10.1021/acs.est.2c08028
Environ. Sci. Technol. 2023, 57, 6636−6646

aqueous pool and finally lead to no isotope fractionation upon the rapid Zn retention by the solids.[26]

4. ENVIRONMENTAL IMPLICATIONS

Various mineral−solution interfacial reactions, including adsorption and substitution, contribute to a "black box" of isotope signals in both experimental and environmental systems. In particular, adsorption and substitution with iron (hydr)oxides play important roles in mediating element geochemical cycling, mobility, and fate, including the isotope fractionation factors of Zn in terrestrial environments. Here, preferential adsorption of heavy Zn isotopes onto FeOOH polymorph surfaces is confirmed in circumneutral pH conditions. Moreover, the present study shows for the first time that isotopically light Zn is incorporated into Fe (hydr)oxide structures. It is recently reported that secondary minerals (e.g., Fe and Mn (hydr)oxides) during pedogenesis enrich light Zn and Cu isotopes as internalized species due to the incorporation of these metals into Fe (hydr)oxides.[4,13] Similarly, the enrichment of light Zn isotopes in acid mine drainage precipitates, jarosite and goethite, relative to the drainage is also attributed to Zn incorporation into the solids.[8] Here, we provide the first experimental evidence for these field observations. We observe larger fractionation factors ($\Delta^{66/64}Zn_{substituted\text{-}stock\ solution}$ = −1.5‰ to −1.2‰) however, for Zn-substituted goethite and lepidocrocite than the theoretical maximum of −0.7‰ for Zn incorporation into Fe (hydr)oxides based on available global soil data[4] and the range of −0.35‰ to −0.08‰ for Zn-substituted goethite.[8] This is probably caused by the different crystal nucleation and growth rates of these Zn-substituted Fe (hydr)oxides under experimental and field conditions[28] and highlights the important role that nucleation and growth processes play in Zn isotope fractionation with Fe (hydr)oxides. Further experimental studies conducted over a range of environmentally relevant conditions (e.g., circumneutral pH, micromolar concentrations of Zn and Fe, and low temperature) and with other minerals are necessary to constrain the theoretical range of Zn isotope fractionation during interactions with Fe (hydr)oxides and further determine the most important processes responsible for Zn isotope fractionation in experimental and natural systems. As an additional implication of this work, the different Zn isotope fractionation directions observed between adsorption onto and incorporation into Fe (hydr)oxides might be used to identify the crystal chemistry of Zn in these minerals according to their Zn isotope compositions. Conclusively, these results reveal possible Zn isotope fractionation mechanisms during mineral−solution geochemical processes pertinent to Earth's critical zone and provide a mechanistic framework toward source tracing and process tracking Zn in contaminated and natural environments.

■ ASSOCIATED CONTENT

Supporting Information

The Supporting Information is available free of charge at https://pubs.acs.org/doi/10.1021/acs.est.2c08028.

Reagent information; details of Zn isotope ratio measurement; powder XRD, TEM, EDS, and zeta potential analyses of obtained minerals; Zn macroscopic adsorption kinetics, adsorption edge, isotherms, and Zn isotope compositions in solid and aqueous phases and mass balance; isotope and chemical compositions of solutions and solids obtained during the Zn substitution experiments; Rietveld structure refinement results of intermediates during Zn-doped FeOOH formation; linear combination fitting analysis of Zn K-edge XANES spectra and structure parameters derived from Zn K-edge EXAFS fitting; Zn species calculation (PDF)

■ AUTHOR INFORMATION

Corresponding Author

Hui Yin − *Key Laboratory of Arable Land Conservation (Middle and Lower Reaches of Yangtse River), Ministry of Agriculture and Rural Affairs, College of Resources and Environment, Huazhong Agricultural University, Wuhan 430070, China;* orcid.org/0000-0003-3060-7025; Phone: +86 27 87280271; Email: yinhui666@mail.hzau.edu.cn; Fax: +86 27 87288618

Authors

Xinran Yan − *Key Laboratory of Arable Land Conservation (Middle and Lower Reaches of Yangtse River), Ministry of Agriculture and Rural Affairs, College of Resources and Environment, Huazhong Agricultural University, Wuhan 430070, China*

Wei Li − *Key Laboratory of Surficial Geochemistry, Ministry of Education, School of Earth Sciences and Engineering, Nanjing University, Nanjing, Jiangsu 210023, China;* orcid.org/0000-0002-0789-0320

Chuanwei Zhu − *State Key Laboratory of Ore Deposit Geochemistry, Institute of Geochemistry, Chinese Academy of Sciences, Guiyang, Guizhou 550002, China*

Caroline L. Peacock − *School of Earth and Environment, University of Leeds, Leeds LS2 9JT, UK*

Yizhang Liu − *State Key Laboratory of Ore Deposit Geochemistry, Institute of Geochemistry, Chinese Academy of Sciences, Guiyang, Guizhou 550002, China*

Hui Li − *Department of Crop and Soil Sciences, North Carolina State University, Raleigh, North Carolina 27695, United States;* orcid.org/0000-0002-9374-5305

Jing Zhang − *Beijing Synchrotron Radiation Facility, Institute of High Energy Physics, Chinese Academy of Sciences, Beijing 100039, China;* orcid.org/0000-0002-3750-374X

Mei Hong − *College of Grassland, Resources and Environment, Inner Mongolia Agricultural University, Hohhot 010018, China*

Fan Liu − *Key Laboratory of Arable Land Conservation (Middle and Lower Reaches of Yangtse River), Ministry of Agriculture and Rural Affairs, College of Resources and Environment, Huazhong Agricultural University, Wuhan 430070, China;* orcid.org/0000-0003-0341-923X

Complete contact information is available at: https://pubs.acs.org/10.1021/acs.est.2c08028

Notes

The authors declare no competing financial interest.

■ ACKNOWLEDGMENTS

The authors gratefully thank the National Natural Science Foundations of China (nos. 42077015, 41771267, 42277392, and 41977288), Key Science and Technology Projects of Inner Mongolia autonomous region (No. 2019ZD001), and the Fundamental Research Funds for the Central Universities

(Grant 103-510320036) and Royal Society Newton Mobility Grant (IEC/NSFC/191423) for financial support.

REFERENCES

(1) Jennings, A. A. Analysis of worldwide regulatory guidance values for the most commonly regulated elemental surface soil contamination. *J. Environ. Manage.* **2013**, *118*, 72−95.
(2) Rout, G. R.; Das, P. Effect of metal toxicity on plant growth and metabolism: I. Zinc. In *Sustainable Agriculture*. Lichtfouse, E.; Navarrete, M.; Debaeke, P.; Véronique, S.; Alberola, C., Eds. Springer Netherlands: Dordrecht; 2009; pp. 873−884, DOI: 10.1007/978-90-481-2666-8_53.
(3) Agency for Toxic Substances and Disease Registry (ATSDR). 2005. *Toxicological profile for zinc*. Atlanta, GA: U.S. Department of Health and Human Services, Public Health Service.
(4) Little, S. H.; Munson, S.; Prytulak, J.; Coles, B. J.; Hammond, S. J.; Widdowson, M. Cu and Zn isotope fractionation during extreme chemical weathering. *Geochim. Cosmochim. Acta* **2019**, *263*, 85−107.
(5) Liu, S. A.; Liu, P. P.; Lv, Y. W.; Wang, Z. Z.; Dai, J. G. Cu and Zn isotope fractionation during oceanic alteration: Implications for oceanic Cu and Zn cycles. *Geochim. Cosmochim. Acta* **2019**, *257*, 191−205.
(6) Zhang, T.; Sun, R. Y.; Liu, Y.; Chen, L.; Zheng, W.; Liu, C. Q.; Chen, J. B. Copper and Zinc isotope signatures in scleratinian corals: Implications for Cu and Zn cycling in modern and ancient ocean. *Geochim. Cosmochim. Acta* **2022**, *317*, 395−408.
(7) Ma, L.; Wang, W.; Xie, M. W.; Wang, W. X.; Evans, R. D. Using Zn isotopic signatures for source identification in a contaminated estuary of Southern China. *Environ. Sci. Technol.* **2020**, *54*, 5140−5149.
(8) Liu, Y. H.; Gao, T.; Xia, Y. F.; Wang, Z. R.; Liu, C. S.; Li, S. H.; Wu, Q. Q.; Qi, M.; Lv, Y. W. Using Zn isotopes to trace Zn sources and migration pathways in paddy soils around mining area. *Environ. Pollut.* **2020**, *267*, No. 115616.
(9) Wang, Z.; Kwon, K. D.; Peacock, C.; Mo, X.; Gou, W.; Feng, X.; Li, W. Zn stable isotope fractionation during adsorption onto todorokite: A molecular perspective from X-ray absorption spectroscopy and density functional theory. *Geochim. Cosmochim. Acta* **2022**, *327*, 116−136.
(10) Guinoiseau, D.; Gélabert, A.; Moureau, J.; Louvat, P.; Benedetti, M. F. Zn isotope fractionation during sorption onto kaolinite. *Environ. Sci. Technol.* **2016**, *50*, 1844−1852.
(11) Mavromatis, V.; González, A. G.; Dietzel, M.; Schott, J. Zinc isotope fractionation during the inorganic precipitation of calcite − Towards a new pH proxy. *Geochim. Cosmochim. Acta* **2019**, *244*, 99−112.
(12) Komárek, M.; Ratié, G.; Vaňková, Z.; Šípková, A.; Chrastný, V. Metal isotope complexation with environmentally relevant surfaces: Opening the isotope fractionation black box. *Crit. Rev. Environ. Sci. Technol.* **2022**, *52*, 3573−3603.
(13) Quantin, C.; Guinoiseau, D. The use of stable isotopes in soil science: Metals. In *Reference Module in Earth Systems and Environmental Sciences*; Elsevier: 2022; pp. 1−8, DOI: 10.1016/B978-0-12-822974-3.00092-6.
(14) Fernandez, A.; Borrok, D. M. Fractionation of Cu, Fe, and Zn isotopes during the oxidative weathering of sulfide-rich rocks. *Chem. Geol.* **2009**, *264*, 1−12.
(15) Opfergelt, S.; Cornélis, J. T.; Houben, D.; Givron, C.; Burton, K. W.; Mattielli, N. The influence of weathering and soil organic matter on Zn isotopes in soils. *Chem. Geol.* **2017**, *466*, 140−148.
(16) Weiss, D. J.; Boye, K.; Caldelas, C.; Fendorf, S. Zinc isotope fractionation during early dissolution of biotite granite. *Soil Sci. Soc. Am. J.* **2014**, *78*, 171−179.
(17) Yan, X. R.; Zhu, M. Q.; Li, W.; Peacock, C. L.; Ma, J. Y.; Wen, H. J.; Liu, F.; Zhou, Z. B.; Zhu, C. W.; Yin, H. Cadmium isotope fractionation during adsorption and substitution with iron (oxyhydr)-oxides. *Environ. Sci. Technol.* **2021**, *55*, 11601−11611.
(18) Pokrovsky, O. S.; Viers, J.; Freydier, R. Zinc stable isotope fractionation during its adsorption on oxides and hydroxides. *J. Colloid Interface Sci.* **2005**, *291*, 192−200.
(19) Juillot, F.; Maréchal, C.; Ponthieu, M.; Cacaly, S.; Morin, G.; Benedetti, M.; Hazemann, J. L.; Proux, O.; Guyot, F. Zn isotopic fractionation caused by sorption on goethite and 2-Lines ferrihydrite. *Geochim. Cosmochim. Acta* **2008**, *72*, 4886−4900.
(20) Gou, W.; Li, W.; Ji, J.; Li, W. Zinc isotope fractionation during sorption onto Al oxides: Atomic level understanding from EXAFS. *Environ. Sci. Technol.* **2018**, *52*, 9087−9096.
(21) Wasylenki, L. E.; Howe, H. D.; Spivak-Birndorf, L. J.; Bish, D. L. Ni isotope fractionation during sorption to ferrihydrite: Implications for Ni in banded iron formations. *Chem. Geol.* **2015**, *400*, 56−64.
(22) Wasylenki, L. E.; Swihart, J. W.; Romaniello, S. J. Cadmium isotope fractionation during adsorption to Mn oxyhydroxide at low and high ionic strength. *Geochim. Cosmochim. Acta* **2014**, *140*, 212−226.
(23) Weiss, D.; Northover, G.; Hanif, M.; García-España, E.; Vilar, R.; Arnold, T.; Markovic, T.; Wissuwa, M.; Delgado, E. Isotope fractionation of zinc in the paddy rice soil-water environment and the role of 2'deoxymugineic acid (DMA) as zincophore under Zn limiting conditions. *Chem. Geol.* **2021**, *577*, No. 120271.
(24) Aucour, A.-M.; Bedell, J.-P.; Queyron, M.; Tholé, R.; Lamboux, A.; Sarret, G. Zn speciation and stable isotope fractionation in a contaminated urban wetland soil−Typha latifolia system. *Environ. Sci. Technol.* **2017**, *51*, 8350−8358.
(25) Nelson, J.; Wasylenki, L.; Bargar, J. R.; Brown, G. E.; Maher, K. Effects of surface structural disorder and surface coverage on isotopic fractionation during Zn(II) adsorption onto quartz and amorphous silica surfaces. *Geochim. Cosmochim. Acta* **2017**, *215*, 354−376.
(26) Skulan, J. L.; Beard, B. L.; Johnson, C. M. Kinetic and equilibrium Fe isotope fractionation between aqueous Fe(III) and hematite. *Geochim. Cosmochim. Acta* **2002**, *66*, 2995−3015.
(27) Clayton, R. E.; Hudson-Edwards, K. A.; Malinovsky, D.; Andersson, P. Fe isotope fractionation during the precipitation of ferrihydrite and transformation of ferrihydrite to goethite. *Mineral. Mag.* **2005**, *69*, 667−676.
(28) Balci, N.; Bullen, T. D.; Witte-Lien, K.; Shanks, W. C.; Motelica, M.; Mandernack, K. W. Iron isotope fractionation during microbially stimulated Fe(II) oxidation and Fe(III) precipitation. *Geochim. Cosmochim. Acta* **2006**, *70*, 622−639.
(29) Guinoiseau, D.; Galer, S. J. G.; Abouchami, W. Effect of cadmium sulphide precipitation on the partitioning of Cd isotopes: Implications for the oceanic Cd cycle. *Earth Planet. Sci. Lett.* **2018**, *498*, 300−308.
(30) Johnson, C. M.; Skulan, J. L.; Beard, B. L.; Sun, H.; Nealson, K. H.; Braterman, P. S. Isotopic fractionation between Fe(III) and Fe(II) in aqueous solutions. *Earth Planet. Sci. Lett.* **2002**, *195*, 141−153.
(31) Hu, B.; Yan, X.; Wang, W.; Li, Y.; Li, H.; Hong, M.; Liu, F.; Yin, H. Iron oxyhydroxide polytype (γ-, δ- and β-FeOOH) structures govern Zn mobility. *Chem. Geol.* **2022**, No. 121167.
(32) Manceau, A.; Nagy, K. L.; Spadini, L.; Ragnarsdottir, K. V. Influence of anionic layer structure of Fe-oxyhydroxides on the structure of Cd surface complexes. *J. Colloid Interface Sci.* **2000**, *228*, 306−316.
(33) Liu, L.; Wang, X.; Zhu, M.; Ma, J.; Zhang, J.; Tan, W.; Feng, X.; Yin, H.; Liu, F. The speciation of Cd in Cd−Fe coprecipitates: Does Cd substitute for Fe in goethite structure? *ACS Earth Space Chem.* **2019**, *3*, 2225−2236.
(34) Gou, W.; Li, W.; Siebecker, M. G.; Zhu, M.; Li, L.; Sparks, D. L. Coupling molecular-scale spectroscopy with stable isotope analyses to investigate the effect of Si on the mechanisms of Zn−Al LDH formation on Al oxide. *Environ. Sci. Technol.* **2022**, *56*, 13829−13836.
(35) Zhu, C.; Liao, S.; Wang, W.; Zhang, Y.; Yang, T.; Fan, H.; Wen, H. Variations in Zn and S isotope chemistry of sedimentary sphalerite, Wusihe Zn-Pb deposit, Sichuan Province China. *Ore Geol. Rev.* **2018**, *95*, 639−648.

https://doi.org/10.1021/acs.est.2c08028
Environ. Sci. Technol. 2023, 57, 6636−6646

(36) Pallavicini, N.; Engström, E.; Baxter, D. C.; Öhlander, B.; Ingri, J.; Rodushkin, I. Cadmium isotope ratio measurements in environmental matrices by MC-ICP-MS. *J. Anal. At. Spectrom.* **2014**, *29*, 1570−1584.
(37) Archer, C.; Andersen, M. B.; Cloquet, C.; Conway, T. M.; Dong, S.; Ellwood, M.; Moore, R.; Nelson, J.; Rehkämper, M.; Rouxel, O.; Samanta, M.; Shin, K.; Sohrin, Y.; Takano, S.; Wasylenki, L. Intercalibration of a proposed new primary reference standard AA-ETH Zn for zinc isotopic analysis. *J. Anal. At. Spectrom.* **2017**, *32*, 415−419.
(38) Wang, Z.-Z.; Liu, S.-A.; Liu, J.; Huang, J.; Xiao, Y.; Chu, Z.-Y.; Zhao, X.-M.; Tang, L. Zinc isotope fractionation during mantle melting and constraints on the Zn isotope composition of Earth's upper mantle. *Geochim. Cosmochim. Acta* **2017**, *198*, 151−167.
(39) Ravel, B.; Newville, M. ATHENA, ARTEMIS, HEPHAESTUS: data analysis for X-ray absorption spectroscopy using IFEFFIT. *J. Synchrotron Radiat.* **2005**, *12*, 537−541.
(40) Kelly, S. D.; Hesterberg, D.; Ravel, B. Analysis of Soils and Minerals Using X-ray Absorption Spectroscopy. In *Methods of Soil Analysis Part 5—Mineralogical Methods*; Soil Science Society of America: 2008; pp. 387−463.
(41) Schauble, E. A. Applying stable isotope fractionation theory to new systems. *Rev. Mineral. Geochem.* **2004**, *55*, 65−111.
(42) Waychunas, G. A.; Fuller, C. C.; Davis, J. A.; Rehr, J. J. Surface complexation and precipitate geometry for aqueous Zn(II) sorption on ferrihydrite: II. XANES analysis and simulation. *Geochim. Cosmochim. Acta* **2003**, *67*, 1031−1043.
(43) Cismasu, A. C.; Levard, C.; Michel, F. M.; Brown, G. E. Properties of impurity-bearing ferrihydrite II: Insights into the surface structure and composition of pure, Al- and Si-bearing ferrihydrite from Zn(II) sorption experiments and Zn K-edge X-ray absorption spectroscopy. *Geochim. Cosmochim. Acta* **2013**, *119*, 46−60.
(44) Aucour, A.; Bedell, J.; Queyron, M.; Magnin, V.; Testemale, D.; Sarret, G. Dynamics of Zn in an urban wetland soil−plant system: Coupling isotopic and EXAFS approaches. *Geochim. Cosmochim. Acta* **2015**, *160*, 55−69.
(45) Frierdich, A. J.; Catalano, J. G. Controls on Fe(II)-activated trace element release from goethite and hematite. *Environ. Sci. Technol.* **2012**, *46*, 1519−1526.
(46) Frierdich, A. J.; Scherer, M. M.; Bachman, J. E.; Engelhard, M. H.; Rapponotti, B. W.; Catalano, J. G. Inhibition of trace element release during Fe(II)-activated recrystallization of Al-, Cr-, and Sn-substituted goethite and hematite. *Environ. Sci. Technol.* **2012**, *46*, 10031−10039.
(47) Trivedi, P.; Axe, L.; Tyson, T. A. An analysis of zinc sorption to amorphous versus crystalline iron oxides using XAS. *J. Colloid Interface Sci.* **2001**, *244*, 230−238.
(48) Roberts, D. R.; Ford, R. G.; Sparks, D. L. Kinetics and mechanisms of Zn complexation on metal oxides using EXAFS spectroscopy. *J. Colloid Interface Sci.* **2003**, *263*, 364−376.
(49) Waychunas, G. A.; Fuller, C. C.; Davis, J. A. Surface complexation and precipitate geometry for aqueous Zn(II) sorption on ferrihydrite I: X-ray absorption extended fine structure spectroscopy analysis. *Geochim. Cosmochim. Acta* **2002**, *66*, 1119−1137.
(50) Bochatay, L.; Persson, P. Metal ion coordination at the water−manganite (γ-MnOOH) interface: II An EXAFS study of zinc(II). *J. Colloid Interface Sci.* **2000**, *229*, 593−599.
(51) Kaur, N.; Gräfe, M.; Singh, B.; Kennedy, B. Simultaneous incorporation of Cr, Zn, Cd, and Pb in the goethite structure. *Clays Clay Miner.* **2009**, *57*, 234−250.
(52) Bryan, A. L.; Dong, S.; Wilkes, E. B.; Wasylenki, L. E. Zinc isotope fractionation during adsorption onto Mn oxyhydroxide at low and high ionic strength. *Geochim. Cosmochim. Acta* **2015**, *157*, 182−197.
(53) Balistrieri, L. S.; Borrok, D. M.; Wanty, R. B.; Ridley, W. I. Fractionation of Cu and Zn isotopes during adsorption onto amorphous Fe(III) oxyhydroxide: Experimental mixing of acid rock drainage and ambient river water. *Geochim. Cosmochim. Acta* **2008**, *72*, 311−328.
(54) Fujii, T.; Moynier, F.; Blichert-Toft, J.; Albarède, F. Density functional theory estimation of isotope fractionation of Fe, Ni, Cu, and Zn among species relevant to geochemical and biological environments. *Geochim. Cosmochim. Acta* **2014**, *140*, 553−576.
(55) Liu, J.; Sheng, A.; Li, X.; Arai, Y.; Ding, Y.; Nie, M.; Yan, M.; Rosso, K. M. Understanding the importance of labile Fe(III) during Fe(II)-catalyzed transformation of metastable iron oxyhydroxides. *Environ. Sci. Technol.* **2022**, *56*, 3801−3811.
(56) Cornell, R. M.; Schwertmann, U. Formation. In *The iron oxides: structure, properties, reactions, occurrences, and uses*, Second ed.; John Wiley & Sons: 2003; pp. 345−364.

https://doi.org/10.1021/acs.est.2c08028
Environ. Sci. Technol. 2023, 57, 6636−6646